Effect of Sintering Temperature and Time on Microstructure and Mechanical Properties of CoCrFeNiMn High-Entropy Alloys

Ning Li , Chengbo Wu , Zhennan Wu , Mengyuan Jiang , Junfeng Hou , Fuyuan Dong *

Posted Date: 25 April 2025

doi: 10.20944/preprints202504.2101.v1

Keywords: high-entropy alloy; discharge plasma sintering; mechanical properties; microstructure

 doi:10.20944/preprints202504.2101.v1

Article

Effect of Sintering Temperature and Time on Microstructure and Mechanical Properties of CoCrFeNiMn High-Entropy Alloys

Ning Li [1,2,3], Chengbo Wu [1], Zhennan Wu [1], Mengyuan Jiang [1], Junfeng Hou [1,2,3] and Fuyuan Dong [1,2,3,*]

[1] School of Materials Science & Engineering, North Minzu University, Yinchuan 750021, China
[2] National and Local Joint Engineering Research Center of Advanced Carbon-Based Ceramics Preparation Technology, Yinchuan 750021, China
[3] Key Lab of Powder Materials & Advance Ceramics, Yinchuan 750021, China
* Correspondence: fydong@alum.imr.ac.cn

Abstract: A single-phase equal-atom five-mdembered High-entropy alloy CoCrFeNiMn was prepared by powder metallurgy. The samples were prepared by discharge plasma sintering technique, and were held at temperatures of 850°C, 950°C, and 1050°C for 5 min, and at temperatures of 1050°C for 3 min, 5 min, and 10 min, respectively. The organization and mechanical properties of the prepared samples were analyzed. The tensile strength and ductility of the alloys gradually increased with the increase of sintering temperature and reached the highest values of 620.0 MPa and 51.0% when the temperature was 1050 °C, respectively. With the increase of holding time, the tensile strength of the alloy gradually decreased and the ductility gradually increased, reaching the highest value of 55.6% when the holding time was 10 minutes. Critical shear stress (τ_0) and normal fracture stress (σ_0) were introduced to analyze the effects of sintering temperature and holding time on tensile strength and fracture mode. The alloy sintered at 1050°C and held for 3 min had the highest hardness value of 191 HV, the best wear resistance, and the wear mechanisms were mainly adhesive and abrasive wear.

Keywords: high-entropy alloy; discharge plasma sintering; mechanical properties; microstructure

1. Introduction

High-entropy alloys (HEAs) have attracted much attention in recent years due to their excellent mechanical properties such as good ductility, excellent fatigue properties, high strength, thermal stability and wear resistance [1–6]. This name refers to the new design concept of alloying by introducing more metal elements. The most famous HEA is the equal mole ratio CoCrFeNiMn alloy, also called Cantor alloy [7,8]. Although it has a complex chemical composition, it forms a simple solid solution phase that gives it exceptional ductility and fracture toughness at high temperatures (~900°C). However, CoCrFeNiMn has relatively low yield and tensile strengths, and this imbalance in mechanical properties limits its potential applications [9,10]. Therefore, it is crucial to improve its strength without introducing additional brittleness.

High-entropy alloys are usually prepared by melting. However, cast High-entropy alloys suffer from compositional segregation, porosity and other casting defects [11,12]. In contrast, powder metallurgy can prepare bulk High-entropy alloys with nano-sized grains, uniform organization and composition, which can significantly improve the mechanical properties of High-entropy alloys. Powder metallurgy can also realize near-final forming of metal parts and improve material utilization. In addition, powder metallurgy can easily add second-phase particles to obtain metal matrix composites.

In this paper, CoCrFeNiMn High-entropy alloy is prepared by powder metallurgy method using discharge plasma sintering furnace. The effects of sintering temperature and holding time on the organization, mechanical properties and wear resistance of CoCrFeNiMn High-entropy alloy are systematically investigated, and the laws of the effects of sintering temperature and holding time on the properties of the alloy are observed.

 doi:10.20944/preprints202504.2101.v1

2. Materials and Methods

The experiments were carried out on High-entropy alloys with nominal composition of $Co_{20}Cr_{20}Fe_{20}Ni_{20}Mn_{20}$ (atomic percentage), in which the alloys were prepared by sintering in a discharge plasma sintering furnace (SPS-20T-10, Shanghai Chenhua Science and Technology Co., Ltd.) at 850°C, 950°C, and 1050°C, with a 5-minute holding time, in which the 1050°C sintered The holding time of the alloy was 3 minutes, 5 minutes and 10 minutes, respectively, and the sintered alloy was a cylinder with a diameter of 25 mm and a height of 8 mm. The sintered samples were subjected to density determination by Archimedes drainage method. The original samples were cut into dog-bone tensile samples and metallographic samples using a BM400-type center-wire cutting machine. The sintered and stretched samples are shown in Figure 1.

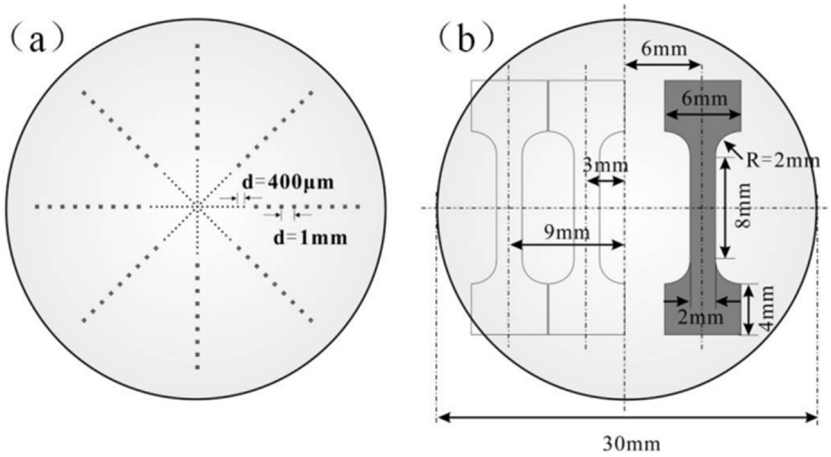

Figure 1. (a) The sintered sample and; (b) stretched sample.

The mechanical properties of the alloy were tested by the CMT5305 universal material testing machine, and the experiment was carried out at room temperature with a tensile rate of 1×10^{-3}mm/s. Three samples of each specimen were taken and stretched under the same process parameters. The wear tester (HT-1000) of Lanzhou Zhongke Kaihua Science and Technology Development Co., Ltd. was used to test the friction and wear properties at room temperature for 15 min, with CoCr15 balls of Φ3 mm, a load of 1000 g, and a sliding speed of 300 rpm. The formula for the wear rate is K = V/P S, where K is the wear rate, V is the wear amount, P is the force loaded in the normal direction, and S is the sliding distance. The microhardness of the sintered samples at different temperatures was measured using a micro Vickers hardness tester (HVS-1000) with a diamond positive tetragonal prism in the indenter, loaded with 9.8 N for 10 s. The microhardness of the alloys at different sintering temperatures and holding times were measured. To measure the microhardness of the alloys, 10 different positions in the samples were selected for measurement to ensure the accuracy of the results. Then, the maximum and minimum values of the data were removed and the average value of the remaining data was taken as the microhardness of the sample. The phase composition was analyzed using an X-ray diffractometer (XRD, XRD-6000 (3KW)) Cu target Kα radiation (tube voltage 40 kV, tube current 30 mA) with a scanning range of 30°~80° and a scanning speed of 4°/mm. The samples of metallographic samples with different sintering temperatures were corroded after grinding and polishing. Optical microscope (OM, ZISS) and scanning electron microscope (SEM, Hitachi TM4000Plusll) were used to observe the microstructure.

3. Results and Discussion

3.1. Microstructure

The XRD diffraction patterns of 850 (sintered at 850°C), 950 (sintered at 950°C), 1050-3 (sintered and held at 1050°C for 3 min), 1050-5 (sintered and held at 1050°C for 5 min), and 1050-10 (sintered and held at 1050°C for 10 min) are shown in Figure 2. It can be seen from the figure that the increase of sintering temperature and holding time did not cause the phase change of CoCrFeNiMn high-entropy alloy, which is still a single-phase FCC structure, and did not form any precipitation phase. The lattice constant and half peak width of the strongest peak (111) of the FCC phase were calculated using Bragg's formula, and the results are shown in Table 1, from which it is easy to see that the FCC

 doi:10.20944/preprints202504.2101.v1

diffraction peaks of the high entropy alloy are shifted to the left because of the increase of the lattice constant of the BCC phase. Since the displacement of the diffraction peak is very small, the change in the lattice constant is not obvious. By observing the half-peak width we can see that the half-peak width gradually increases as the sintering temperature increases. This is mainly due to the increase in temperature, the full diffusion of elements, and the increase in internal defects after the alloy is densified. With the increase of holding time, the half peak width gradually increases, mainly because of grain growth, and alloy internal stress reduction caused by.

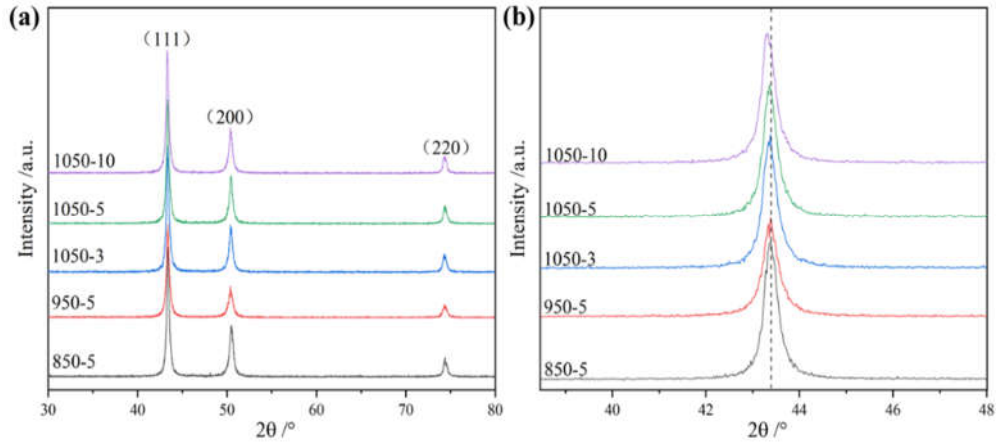

Figure 2. X-ray diffraction pattern: (a) original drawing; (b) local enlargement.

Table 1. Lattice constant and half peak width.

Sample	a /(Å)	FWHM
850	0.3882	0.40395
950	0.3883	0.41390
1050-3	0.3884	0.43123
1050-5	0.3885	0.42526
1050-10	0.3887	0.42302

The experimental grain size was measured using Image-pro-plus software. Figure 3 shows the alloy grain size sintered at different temperature sintering temperatures. From the figure, it can be seen that when the sintering temperature is 850°C, the alloy grain size reaches a minimum of about 18.11 μm, which is because the internal particles of the alloy heat themselves uniformly under the action of Joule heat during plasma sintering, and the atoms on the surface of the particles are in the activation state, so the process of sintered body densification avoids the uneven densification of the alloy caused by the heat transfer from the outside to the inside, which leads to the refinement of the grains. With the gradual increase in temperature and holding time, the grain size of the alloy increases gradually, which is attributed to the increased diffusion driving force at higher temperatures leading to grain growth, but the degree of grain growth is not high. The SEM micrographs of the alloy are shown in Figure 4, the whole specimen shows an equiaxial grain structure and a large number of twins exist in it. When the sintering temperature was 850°C, the pores of the alloy were obvious, and the low sintering temperature resulted in the alloy having inconspicuous grain boundaries and low actual density. With the increase of sintering temperature and holding time, the pores in the alloy are gradually reduced and the density of the alloy is gradually increased, the actual density of the alloy is shown in Figure 5, and the relative density value of the alloy is the largest when the sintering temperature is 1050 ℃ and the holding time is 10 minutes. Figure 6 shows the measured values of microhardness of the samples after different sintering temperatures and holding times. The results show that the hardness of the alloy gradually increases with the increase of sintering temperature and decreases with the extension of holding time, and the hardness value is the highest at 191 HV when the sintering temperature is 1050°C and the holding time is 3 min. This is since the diffusion and fusion of alloying elements are more fully integrated with the increase of the sintering temperature, the internal pores of the alloy are reduced, and the densification is improved. With the extension

 doi:10.20944/preprints202504.2101.v1

of the holding time, the alloy grain size gradually increases and the resistance to deformation decreases, leading to a decrease in hardness.

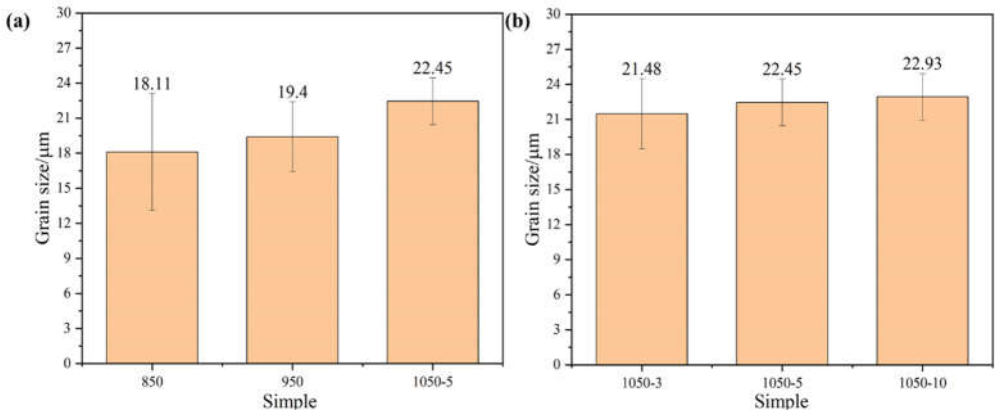

Figure 3. Average grain size of high entropy alloy: (a) sintered at different sintering temperatures; (b) sintered at different holding times.

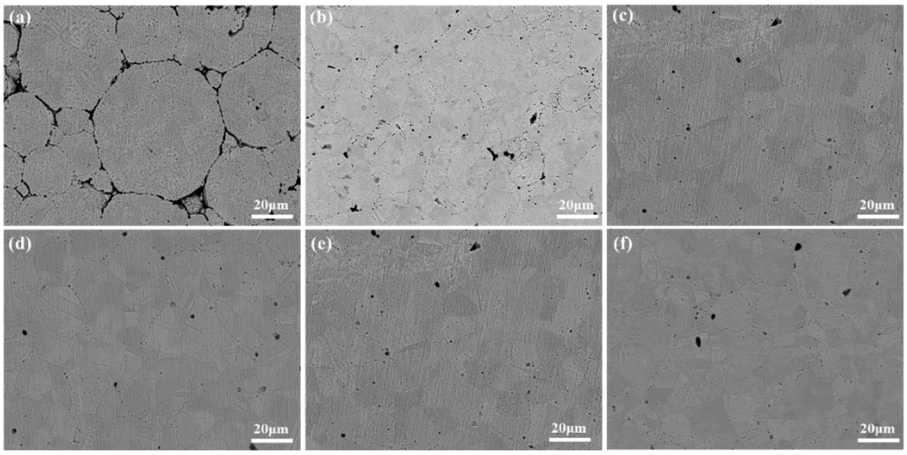

Figure 4. SEM images of alloys at different sintering temperatures: (a) 850; (b) 950; (c) 1050-5; (d) 1050-3; (e) 1050-5; (f) 1050-10.

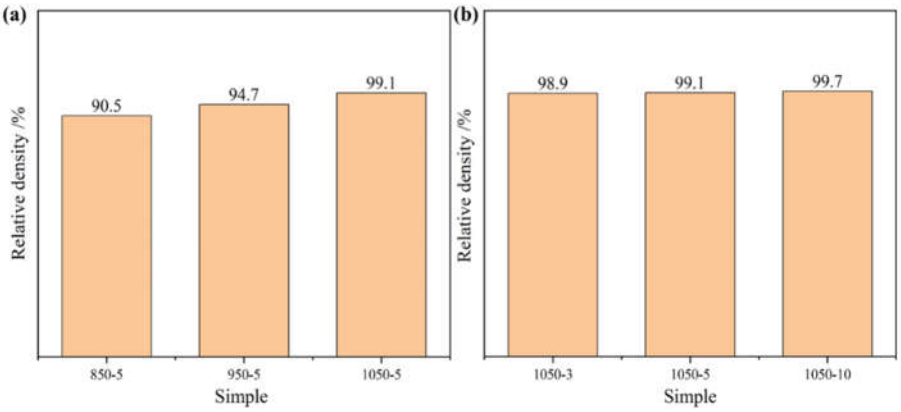

Figure 5. High entropy alloy relative density: (a) sintered at different sintering temperatures; (b) sintered at different holding times.

 doi:10.20944/preprints202504.2101.v1

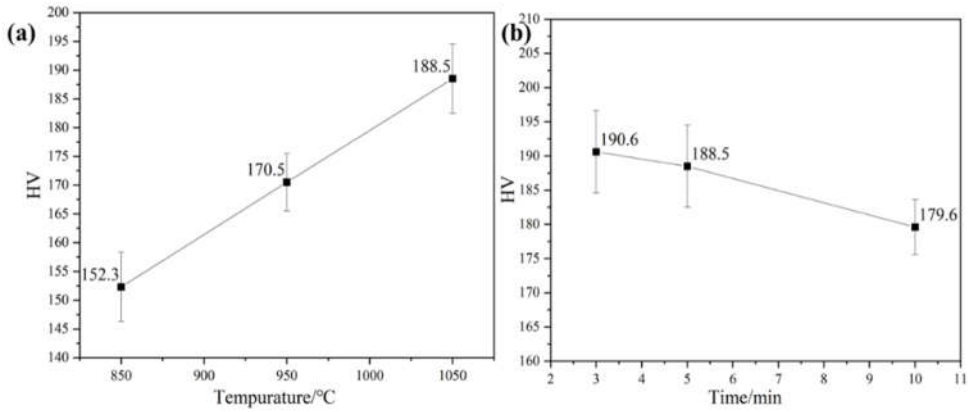

Figure 6. Hhardness: (a) sintered at different sintering temperatures; (b) sintered at different holding times.

3.2. Mechanical Properties

Figure 7 shows the room temperature tensile engineering stress-strain curve and true stress-strain curve of High-entropy alloy sintered at different sintering temperatures and holding times, from which it is learned that the strength and ductility of the alloy gradually increases with the increase of temperature, and the strength of the alloy gradually decreases and the ductility gradually increases with the increase of holding time. When the temperature is 850 ℃, the tensile strength and plasticity of the alloy is only 358.3 MPa and 9.1%, this is due to the existence of a large number of pores in the alloy sintered at 850 ℃, the densification is very poor, and the sintering temperature is too low resulting in the elements can not be sufficiently diffused, the particles can not be completely combined, resulting in poor tensile properties [13]. The strength of the alloy reaches its maximum value of 629.0 MPa when the holding time is 3 minutes at a temperature of 1050°C. The ductility of the alloy reaches its maximum value of 55.6% when the holding time is 10 minutes at a temperature of 1050°C. The ductility of the alloy reaches its maximum value of 55.6% when the holding time is 10 minutes at a temperature of 1050°C. This is because as the holding time increases, the grain boundary energy decreases and the grain growth leads to an increase in ductility and a decrease in strength. The tensile strength and elongation do not change much due to low grain growth.

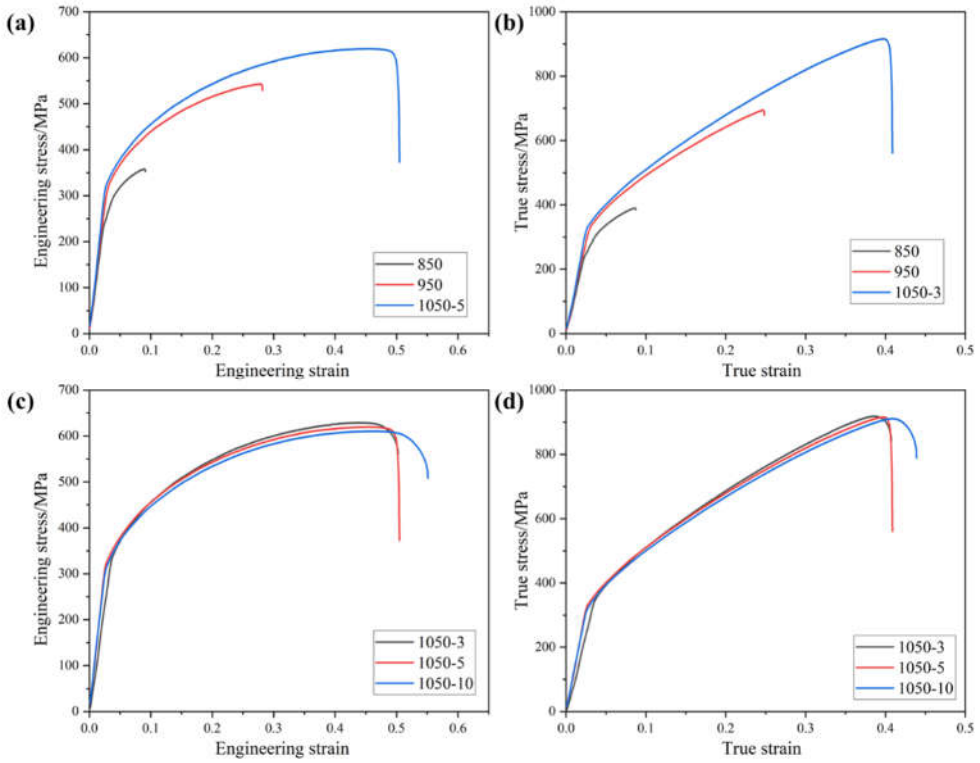

Figure 7. Tensile (a) (c) engineering stress-strain curves and (b) (d) true stress-strain curves of high entropy alloys sintered at different sintering temperatures and holding times at room temperature.

 doi:10.20944/preprints202504.2101.v1

Figure 8 shows the yield strength, tensile strength and elongation graphs, which can be more intuitively seen as trend of the yield strength, tensile strength and elongation of the alloy with the increase in temperature and holding time. Through the different sintering temperatures and different holding times sintered alloy strength and elongation of linear fitting to get the fitted line segment shown in Figure 9, can be seen in a certain sintering temperature and holding time within the temperature and holding time with the increase in temperature and the extension of the holding time, tensile strength and elongation has a certain regularity. When the sintering temperature is increased from 850°C to 1050°C, the tensile strength and elongation of the alloy show a linearly increasing trend. When the holding time was increased from 3 minutes to 10 minutes, the alloy tensile strength showed a linear decreasing trend and the elongation showed a linear increasing relationship.

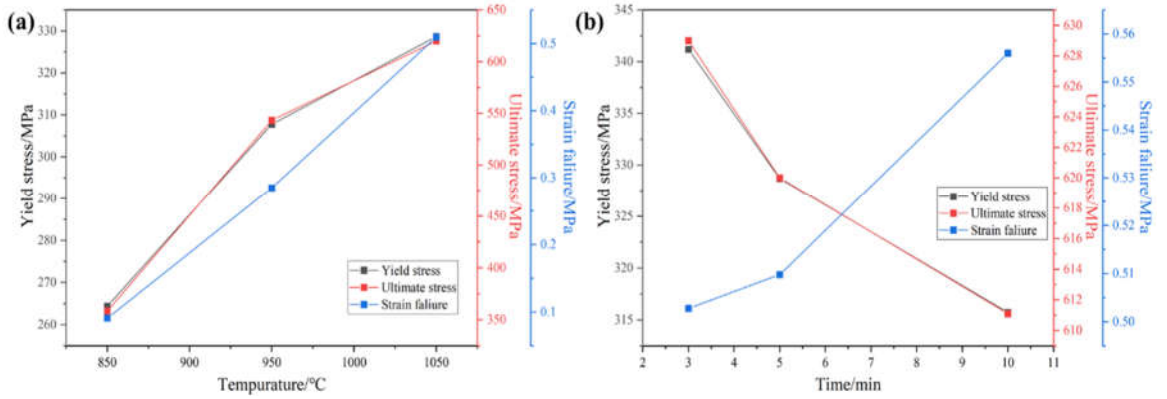

Figure 8. Yield strength, tensile strength and elongation: (a) sintered at different sintering temperatures; (b) sintered at different holding times.

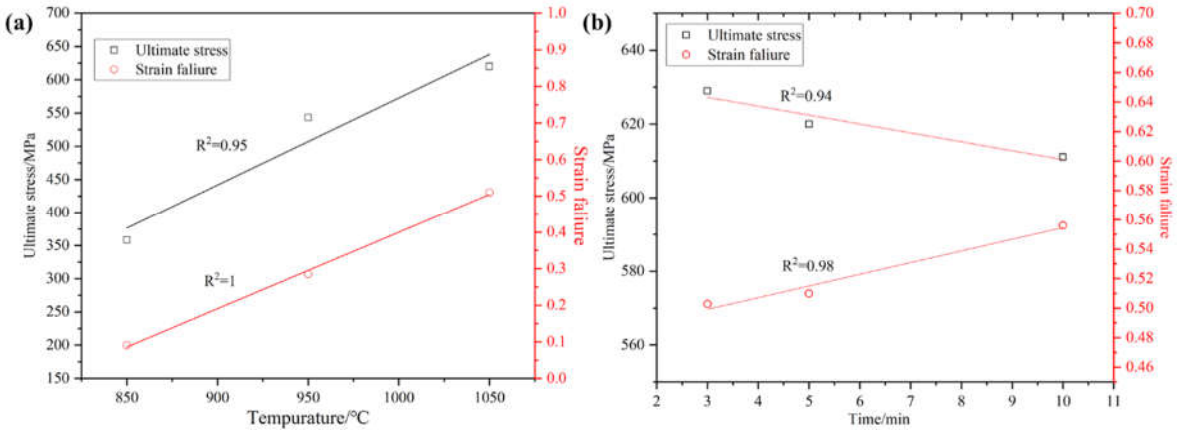

Figure 9. (a) Strength and elongation trends of the high entropy alloy with different sintering temperatures and (b) different holding times.

The difference in tensile fracture angle of the prepared samples at different sintering temperatures is shown in Fig. 10(a). As the sintering temperature increases from 850°C to 1050°C, the fracture break angle of the tensile samples decreases gradually. When the sintering temperature is 850°C, the tensile sample has the largest fracture angle of 81°. When the sintering temperature was 950°C and 1050°C, the fracture angles of the tensile samples were 73° and 53°, respectively. The fitting analysis was carried out by using origin software, and the results showed that the fracture angle of the sample decreased gradually with the increase of sintering temperature, which was fitted by using the formula y=86.33-5.33*exp((x-850)/109.14)), and the fitting R^2=1, which indicated that the fitting effect was good. The difference in tensile fracture angle of the samples prepared at 1050°C after different holding times is shown in Fig. 11(a). As the holding time increases from 3 min to 10 min, the fracture break angle of the tensile samples decreases gradually. When the holding time is 3 min, the tensile samples have the largest fracture angle of 55°. When the holding time was 5 min and 10 min, the fracture angle of the tensile samples was 53° and 50°, respectively. Continuing to fit the value of the tensile fracture angle analysis, the results show that with the increase of the insulation time, the sample fracture angle

 doi:10.20944/preprints202504.2101.v1

gradually decreases, using the formula y = 60.08 * x - 0.08 to fit it, the fitting R^2 = 0.99, indicating that the fitting effect is good.

Zhang and Eckert [14] proposed an elliptic criterion to analyze the fracture behavior of bulk metallic glasses (BMGs), introducing parameters related to this material to explain the deformation and damage behavior of different undercuts [15],expressed as follows:

$$\left(\frac{\sigma}{\sigma_0}\right)^2 + \left(\frac{\tau}{\tau_0}\right)^2 = 1, \tag{1}$$

where σ and τ are the normal and shear stresses applied on the same plane, σ_0 and τ_0 are the critical normal and shear fracture strengths, respectively, and $\alpha = \sigma_0/\tau_0$ is the fracture mode factor. When the tensile stress τ_T is applied to the sample, the normal stress σ and shear stress τ on any shear surface can be expressed as:

$$\sigma = \sigma_F \sin^2 \theta_T, \tag{2}$$

$$\tau = \sigma_F \sin \theta_T \cdot \cos \theta_T, \tag{3}$$

Combining the above formulas, the fracture mode factor α can be expressed as a function of the tensile fracture angle θ_T, σ_0 and τ_0 can be expressed as a function of the tensile fracture strength σ_F and α:

$$\alpha = \sqrt{\frac{1}{2}}(1 - \cot^2 \theta_T), \tag{4}$$

$$\tau_0 = \frac{\sigma_F}{2\sqrt{1-\alpha^2}}, \tag{5}$$

$$\tau_0 = \frac{\sigma_F}{2\alpha\sqrt{1-\alpha^2}}, \tag{6}$$

Without considering the effect of necking behavior, the tensile shear fracture angle is mainly determined by the parameter α. The graphs of σ_0 and τ_0 functions are calculated by the equations of (4)-(6) [16].

The plots of σ_0 and τ_0 functions for the samples prepared at 850°C, 950°C and 1050°C sintering temperatures, respectively, are shown in Figure 10(b). From the Figure, it can be seen that with the increase of sintering temperature, the critical normal fracture strength σ_0 shows a gradually increasing trend, and the selection of the formula $y = 4.55*x^{4.76}$ to fit it found that the fitting R^2 = 0.99, the fitting effect is good. The shear fracture strength τ_0 firstly rises and then gradually tends to level off, and y=-2.15+1.07*(1-exp(-x/62.15))+1.07*(1-exp(-x/62.15))+1.07*(1-exp(-x/62.15)) is chosen to fit it, and the fitting R^2=1, which is a good fitting effect. From the critical normal fracture strength σ_0 and shear fracture strength τ_0 fitting images, it can be seen that with the increase of sintering temperature, the critical normal fracture strength σ_0 shows an obvious rising trend, and when the sintering temperature reaches a certain temperature, the shear fracture strength τ_0 no longer rises, resulting in a gradual decrease in the tensile fracture angle. The plots of σ_0 and τ_0 functions for the samples prepared at 3 min, 5 min and 10 min holding time, respectively, are shown in Figure 11(b). From the Figure, it can be seen that with the increase of holding time, the critical normal fracture strength σ_0 shows a gradual increase in the trend, the selection of the formula y = 56.53 * exp (-x/-5.71) + 959.13 to fit it found that the fitting R^2 = 0.99, the fitting effect is good. The shear fracture strength τ_0 shows a gradual decrease, and y=620.41-64.68*(1-exp(-x/2.63))-64.68*(1-exp(-x/2.63)) is chosen to fit it, and the fitting R^2=0.99, the fitting effect is good. From the critical normal fracture strength σ_0 and shear fracture strength τ_0 fitting images, it can be seen that with the increase of holding time, the critical normal fracture strength σ_0 shows a significant rising trend, while the shear fracture strength τ_0 shows a gradual decline in the trend of the rise of the critical normal fracture strength σ_0 and the decline of the shear fracture strength τ_0 leads to a gradual decrease in the tensile fracture angle. With the increase of sintering temperature and holding time, the High-entropy alloy sample gradually tends to be dense, the reduction of alloy pores, the full diffusion of elements and the full combination of particles are the main reasons for the rise of σ_0, and the final sample fracture mode gradually evolves from forward fracture to shear fracture.

 doi:10.20944/preprints202504.2101.v1

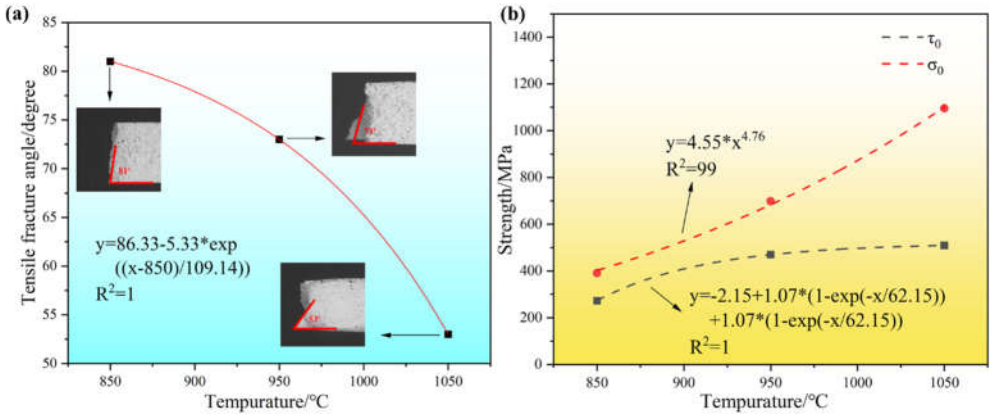

Figure 10. Different sintering temperatures: (a) Relationship of tensile shear fracture angle with the increase of the equivalent strain; (b) variations in τ_0 and σ_0 as a function of the imposed strain.

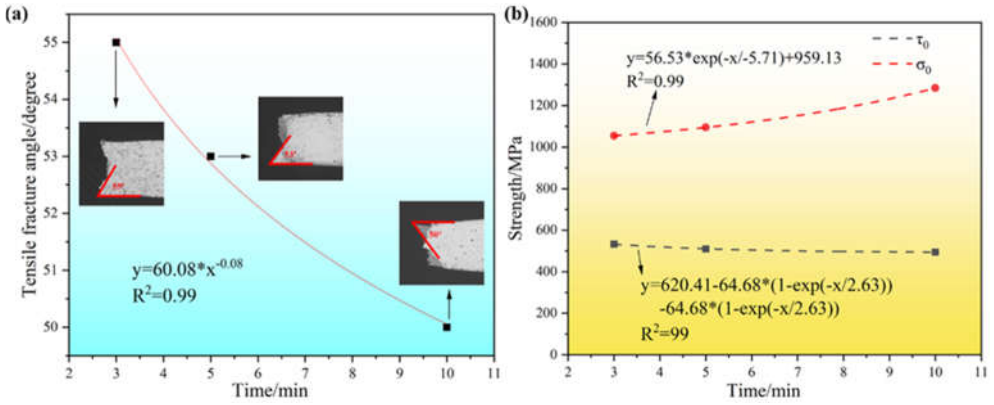

Figure 11. Different holding times: (a) Relationship of tensile shear fracture angle with the increase of the equivalent strain; (b) variations in τ_0 and σ_0 as a function of the imposed strain.

Figure 12 shows the true stress-strain versus strain-hardening curves of High-entropy alloy samples prepared at different sintering temperatures and holding times. From Figure 12(a), it can be seen that in the sintered samples prepared at 850 ℃ in the low strain region strain hardening rate is very fast, with the continuation of stretching, the strain rate gradually slowed down and then continued to decline rapidly until the tensile samples fracture. The samples prepared by sintering at 950°C also show three stages, firstly a rapid decline, followed by a leveling off and finally a continued rapid decline. There is a slight increase in the work-hardening region compared to the sintered samples prepared at 850 °C. The samples prepared by sintering at 1050°C show three stages of rapid decline, followed by a slow increase and finally a continued rapid decline. Compared to the samples prepared by sintering at 850°C and 950°C, the work-hardening region increases significantly, which is mainly due to the reduction of internal pores, more homogeneous bonding between elements, and the generation of twins in the High-entropy alloys as the temperature increases. From Figure 12(b), it can be seen that the samples prepared under the holding time of 3min, 5min and 10min respectively show three stages of rapid decrease, then slow increase and finally rapid decrease. The intersection of the stress-strain curves and strain-hardening curves of the three samples occurred at higher strains. The intersection of the true stress-strain curves of the samples prepared at a holding time of 3 min is slightly lower than that of the samples prepared at a holding time of 5 min, and both intersections are lower than that of the samples prepared at a holding time of 5 min. Due to the delay of necking, the ductility of the samples prepared with a holding time of 10 min is the highest and the ductility of the samples prepared with a holding time of 3 min is the worst.

Figure 13 shows the fractured picture of the sintered alloy under different sintering temperatures and holding times, from Figure (a) it can be seen that when the sintering temperature is 850 ℃, the elemental particles are obviously not completely fused, the elemental diffusion is not uniform, resulting in poor performance of tensile strength and elongation, with the sintering temperature increased to 950 ℃ elemental fusion is more fully, there are a small number of tough nests appear, but still

 doi:10.20944/preprints202504.2101.v1

presents a certain amount of particles and cracks, when the temperature is increased to 1050 ℃, the elemental fusion is more fully, the tough nests increased significantly, with the prolongation of the holding time, the performance of the tough nests is more pronounced.

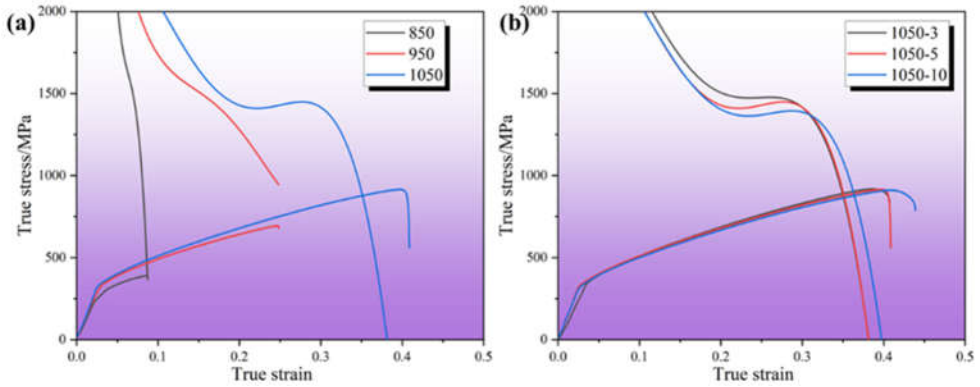

Figure 12. Strain hardening curves of high entropy alloy: (a) sintered at different sintering temperatures; (b) sintered at different holding times.

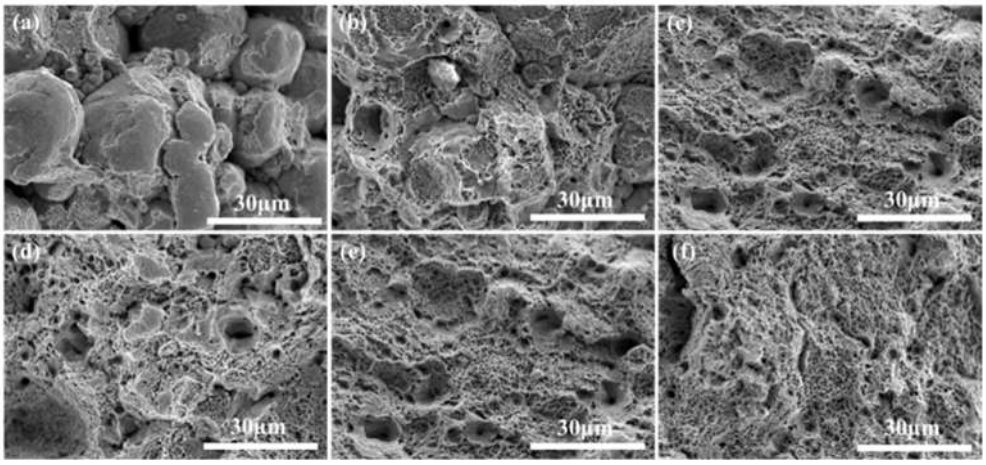

Figure 13. High entropy alloy fracture: (a) 850; (b) 950 (c); 1050-5; (d) 1050-3; (e) 1050-5; (f) 1050-10.

3.3. Wear Properties

Figure 14 shows the friction coefficient-time curves of sintered alloys at different sintering temperatures and holding times. From the Figure, it can be seen that at the beginning of the test, the interface is very rough and the contact area with the grinding ball is very small. When the grinding ball is worn, a cold welding effect occurs, which requires a large shear force to cut it, causing the friction coefficient to increase rapidly [17]. With the increase of wear time, the contact area increases and the interface becomes a smooth friction layer, so that the friction coefficient gradually stabilizes. The friction coefficients of the samples under different conditions in the Figure show large fluctuations, which are mainly due to the periodic accumulation and elimination of wear debris from the wear surface [18,19]. The friction coefficient increases with the accumulation of wear debris on the wear surface. The coefficient of friction decreases when the wear debris separates from the wear surface or fills in the cracks. Among them, porosity in alloys 850 and 950 caused localized fractures. Therefore, the localized fracture caused by porosity is the reason for the large fluctuation of friction coefficient [17–20].

Figure 15 shows the average friction coefficient and wear rate of the sintered alloy at different sintering temperatures and holding times. It can be seen from Figure 15 (a) that the average friction coefficient and wear rate of the alloy show a downward trend with the increase of sintering temperature. It can be seen from Figure 15 (b) that with the increase of holding time, the average friction coefficient and wear rate of the alloy increase slightly and remain basically unchanged. Figure 16 shows the wear surface of the alloy after room temperature frictional wear. It can be seen from the Figure that the samples sintered at different temperatures and holding times have similar wear morphology, including certain scratches and steps. Some plastic deformation exists in the direction

 doi:10.20944/preprints202504.2101.v1

parallel to the scratches, and when the plastic deformation of the alloy exceeds a certain level, the alloy cracks and breaks into wear chips. As wear proceeds, some of the chips undergo fragmentation, accumulation, and elimination. Finally they are compacted to form steps. Another portion of the debris peels off from the worn surface and becomes crumbs [20]. Slight oxidation of the wear surface can be observed from the Figure, and obvious grooves can also be observed from the Figure, so the wear mechanism of this alloy is adhesive wear.

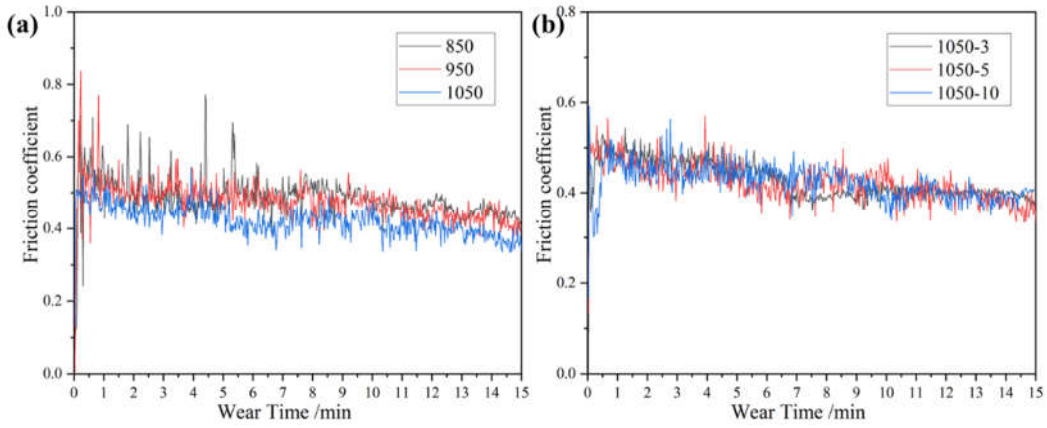

Figure 14. Friction coefficient of high entropy alloy: (a) sintered at different sintering temperatures; (b) sintered at different holding times.

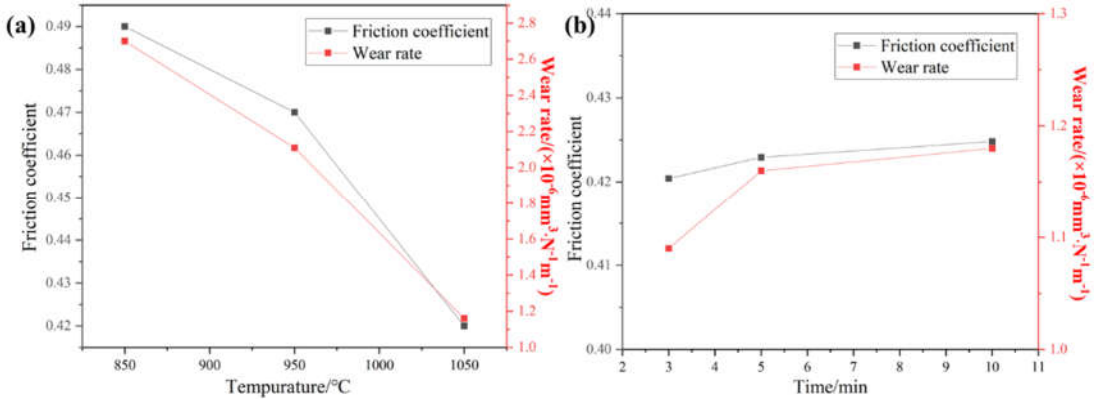

Figure 15. Average friction coefficient and wear rate: (a) sintered at different sintering temperatures; (b) sintered at different holding times.

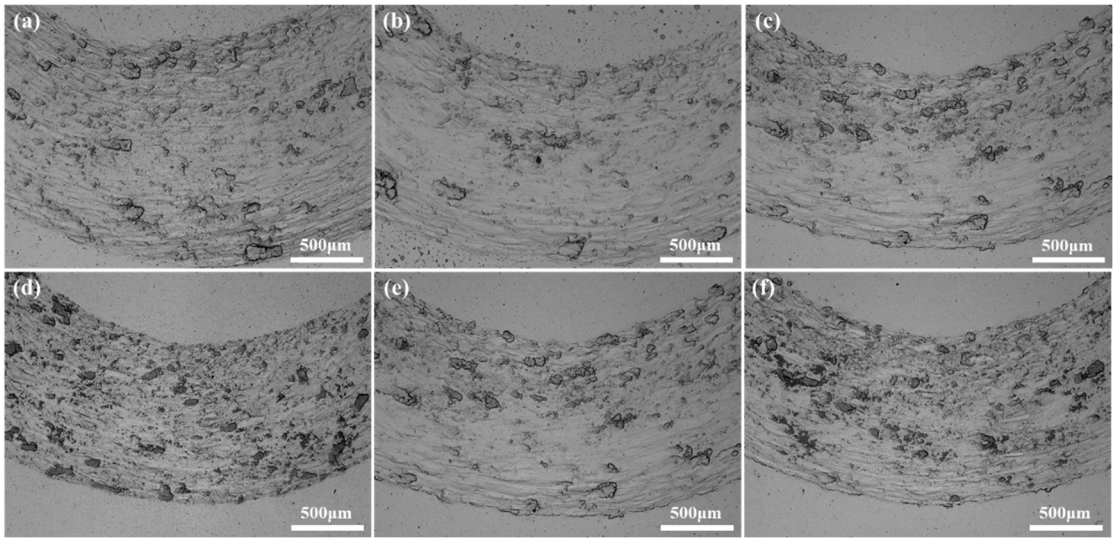

Figure 16. Wear morphology of high entropy alloy sintered at different sintering temperatures and holding times: (a) 850 (b) 950 (c) 1050-5 (d) 1050-3 (e) 1050-5 (f) 1050-10.

 doi:10.20944/preprints202504.2101.v1

4. Conclusions

In this study, we successfully sintered CoCrFeNiMn High-entropy alloy powder with SPS. The microstructure and mechanical properties of CoCrFeNiMn High-entropy alloy were investigated at different sintering temperatures and holding times. The following conclusions can be drawn.

(1) The alloy sintered at 1050°C and held for 3 min has the highest tensile strength of 629.0 MPa, and the alloy sintered at 1050°C and held for 10 min has the best ductility of 55.6%. The fracture mechanism was a ductile fracture.

(2) As the sintering temperature increases, the porosity of the alloy decreases and the tensile properties and ductility increase. With the increase of holding time, the tensile strength of the alloy decreases, the grain size increases and the ductility rises.

(3) With the increase of sintering temperature, the critical normal fracture strength σ_0 shows an obvious rising trend, and when the sintering temperature reaches a certain temperature, the shear fracture strength τ_0 no longer rises. With the increase of holding time, the critical normal fracture strength σ_0 shows a clear rising trend, and the shear fracture strength τ_0 shows a gradual decline. The alloy fracture form is gradually changed from normal fracture to shear fracture mode.

(4) The alloy sintered at 1050°C and held for 3 minutes has the highest hardness and the best wear resistance, and the wear mechanism is mainly adhesive wear and abrasive wear.

Author Contributions: Conceptualization, N.L. and F.D.; Methodology, J.H. and Z.W.; Software, Z.W.; Validation, M.J. and J.H.; Investigation, C.W.; Writing—original draft preparation, N.L. and C.W.; Writing—review and editing, F.D.; Supervision, F.D. All authors have read and agreed to the published version of the manuscript.

Funding: The authors thank the financial support of the Ningxia Natural Science Foundation (No.2023AAC03289).

Data Availability Statement: Data will be made available on request.

Conflicts of Interest: The authors declare no conflicts of interest.

References

1. Li, D.; Li, C.; Feng, T.; Zhang, Y.; Sha, G.; Lewandowski, J.J.; Liaw, P.K.; Zhang, Y. High-entropy Al0.3CoCrFeNi alloy fibers with high tensile strength and ductility at ambient and cryogenic temperatures. *Acta Mater.* **2017**, *123*, 285–294, https://doi.org/10.1016/j.actamat.2016.10.038.
2. Zhou, Y.J.; Zhang, Y.; Wang, Y.L.; Chen, G.L. Solid solution alloys of AlCoCrFeNiTix with excellent room-temperature mechanical properties. *Appl. Phys. Lett.* **2007**, *90*, 181904, https://doi.org/10.1063/1.2734517.
3. Chen, J.; Zhou, X.; Wang, W.; Liu, B.; Lv, Y.; Yang, W.; Xu, D.; Liu, Y. A review on fundamental of high entropy alloys with promising high–temperature properties. *J. Alloy. Compd.* **2018**, *760*, 15–30, https://doi.org/10.1016/j.jallcom.2018.05.067.
4. Whitfield, T.E.; Pickering, E.J.; Owen, L.R.; Senkov, O.N.; Miracle, D.B.; Stone, H.J.; Jones, N.G. An assessment of the thermal stability of refractory high entropy superalloys. *J. Alloy. Compd.* **2021**, *857*, https://doi.org/10.1016/j.jallcom.2020.157583.
5. Chuang, M.-H.; Tsai, M.-H.; Wang, W.-R.; Lin, S.-J.; Yeh, J.-W. Microstructure and wear behavior of AlxCo1.5CrFeNi1.5Tiy high-entropy alloys. *Acta Mater.* **2011**, *59*, 6308–6317, https://doi.org/10.1016/j.actamat.2011.06.041.
6. Hemphill, M.; Yuan, T.; Wang, G.; Yeh, J.; Tsai, C.; Chuang, A.; Liaw, P. Fatigue behavior of Al0.5CoCrCuFeNi high entropy alloys. *Acta Mater.* **2012**, *60*, 5723–5734, https://doi.org/10.1016/j.actamat.2012.06.046.
7. Cantor B , Chang I T H , Knight P .Microstructural development in equiatomic multicomponent alloys.Materials Science & Engineering, A. Structural Materials: Properties, Misrostructure and Processing, 2004:A375/377.
8. Otto, F.; Yang, Y.; Bei, H.; George, E. Relative effects of enthalpy and entropy on the phase stability of equiatomic high-entropy alloys. *Acta Mater.* **2013**, *61*, 2628–2638, https://doi.org/10.1016/j.actamat.2013.01.042.
9. Pickering, E.; Muñoz-Moreno, R.; Stone, H.; Jones, N. Precipitation in the equiatomic high-entropy alloy CrMnFeCoNi. *Scr. Mater.* **2016**, *113*, 106–109, https://doi.org/10.1016/j.scriptamat.2015.10.025.

 doi:10.20944/preprints202504.2101.v1

10. Otto, F.; Dlouhý, A.; Somsen, C.; Bei, H.; Eggeler, G.; George, E.P. The influences of temperature and microstructure on the tensile properties of a CoCrFeMnNi high-entropy alloy. *Acta Mater.* **2013**, *61*, 5743–5755, doi:10.1016/j.actamat.2013.06.018.
11. Dong, Y.; Yao, Z.; Huang, X.; Du, F.; Li, C.; Chen, A.; Wu, F.; Cheng, Y.; Zhang, Z. Microstructure and mechanical properties of AlCoxCrFeNi3-x eutectic high-entropy-alloy system. *J. Alloy. Compd.* **2020**, *823*, https://doi.org/10.1016/j.jallcom.2020.153886.
12. Dong, Y.; Jiang, L.; Jiang, H.; Lu, Y.; Wang, T.; Li, T. Effects of annealing treatment on microstructure and hardness of bulk AlCrFeNiMo0.2 eutectic high-entropy alloy. *Mater. Des.* **2015**, *82*, 91–97, https://doi.org/10.1016/j.matdes.2015.05.046.
13. Cheng H , Xie Y C , Tang Q H ,et al.Microstructure and mechanical properties of FeCoCrNiMn high-entropy alloy produced by mechanical alloying and vacuum hot pressing sintering.中国有色金属学报(英文版), 2018.
14. Zhang Z F , Eckert J .Unified Tensile Fracture Criterion.Physical review letters, 2005, 94(9):p.094301.1-094301.4.DOI:0031-9007(2005)94:9<094301.1:UTFC>2.0.TX;2-A.
15. Zhiyu ZhangGerardo PerozzielloPaolo BoccazziAnthony J. SinskeyOliver GeschkeKlavs F. Jensen.Microbioreactors for Bioprocess Development.JALA: Journal of the Association for Laboratory Automa-tion, 2007, 12(3).
16. Dong, F.; Zhang, P.; Pang, J.; Ren, Y.; Yang, K.; Zhang, Z. Strength, damage and fracture behaviors of high-nitrogen austenitic stainless steel processed by high-pressure torsion. *Scr. Mater.* **2014**, *96*, 5–8, https://doi.org/10.1016/j.scriptamat.2014.09.016.
17. Fang, Y.; Chen, N.; Du, G.; Zhang, M.; Zhao, X.; Cheng, H.; Wu, J. High-temperature oxidation resistance, mechanical and wear resistance properties of Ti(C,N)-based cermets with Al0.3CoCrFeNi high-entropy alloy as a metal binder. *J. Alloy. Compd.* **2020**, *815*, https://doi.org/10.1016/j.jallcom.2019.152486.
18. Joseph, J.; Haghdadi, N.; Shamlaye, K.; Hodgson, P.; Barnett, M.; Fabijanic, D. The sliding wear behaviour of CoCrFeMnNi and AlxCoCrFeNi high entropy alloys at elevated temperatures. *Wear* **2019**, *428-429*, 32–44, https://doi.org/10.1016/j.wear.2019.03.002.
19. Chen, MingLan, LiweiShi, XiaohuiYang, HuijunZhang, MinQiao, Junwei.The tribological properties of Al0.6CoCrFeNi high-entropy alloy with the sigma phase precipitation at elevated temperature.Journal of Alloys and Compounds: An Interdisciplinary Journal of Materials Science and Solid-state Chemistry and Physics, 2019, 777.
20. Wu, J.-M.; Lin, S.-J.; Yeh, J.-W.; Chen, S.-K.; Huang, Y.-S.; Chen, H.-C. Adhesive wear behavior of AlxCoCrCuFeNi high-entropy alloys as a function of aluminum content. *Wear* **2006**, *261*, 513–519, https://doi.org/10.1016/j.wear.2005.12.008.